We are IntechOpen,
the world's leading publisher of
Open Access books
Built by scientists, for scientists

6,900
Open access books available

185,000
International authors and editors

200M
Downloads

154
Countries delivered to

Our authors are among the

TOP 1%
most cited scientists

12.2%
Contributors from top 500 universities

BOOK CITATION INDEX CLARIVATE ANALYTICS INDEXED

WEB OF SCIENCE™

Selection of our books indexed in the Book Citation Index
in Web of Science™ Core Collection (BKCI)

Interested in publishing with us?
Contact book.department@intechopen.com

Numbers displayed above are based on latest data collected.
For more information visit www.intechopen.com

The Laboratorial Research of Two-Phase Free Convection Devices for Cooling of Materials and Industrial Machines

Yakov B. Gorelik and Artur H. Khabitov

Abstract

Refrigeration systems based on free convection (two-phase thermosyphons) are used for cooling equipment units in chemical, nuclear power, and steel-making industries, as well as for thermal stabilization of natural materials with temperature-dependent properties, such as permafrost. Results of laboratory testing are reported for two types of thermosyphons applied mainly to the thermal stabilization of frozen ground: (a) vertical tubes with finning and (b) systems with horizontal evaporation tubes (HET systems). Their uses are currently restricted to relatively small thermal loads, but the effect of the loads on the cooling performance remains poorly investigated. Theoretical analysis of internal and external heat transfer in a vertical thermosyphon provides constraints on the boundary conditions at the evaporator wall, to be used in formulating and solving problems on the temperature regime of frozen ground stabilized with thermosyphons. Comparison of measured and calculated parameters that characterize the operation of a model HET system allows improving the calculation quality by applying the respective corrections.

Keywords: thermosyphons, refrigeration systems, free convection, two-phase flow, hydraulic resistance, cooling effect, experimental modeling, theoretical modeling, permafrost

1. Introduction

Refrigeration systems based on free convection (two-phase thermosyphons) are used for cooling equipment units in chemical, nuclear power, and steel-making industries, as well as for the thermal stabilization of natural materials with temperature-dependent properties, such as permafrost. Thermosyphons (also called "heat pipes" [1]) have different design features and sizes depending on application and operation conditions [1, 2]. Generally, two-phase thermosyphons consist of an evaporator and a condenser. The evaporator has a tightly closed case partly filled with liquid working fluid (coolant) and is placed in immediate vicinity of the cooled equipment or inside the cooled ground. The condenser contacts with a colder ambience (e.g., atmospheric air) and gives up heat. Heat flux to the evaporator boils up the fluid, and the released vapor moves to the condenser driven by the saturation

vapor pressure gradient. The vapor condenses in the condenser, releasing heat into the environment, while the liquid phase of the fluid returns into the evaporator driven by gravity, capillary, or other forces, and the cycle repeats. The capillary liquid flow is provided by special microcellular lining on the inner walls of the thermosyphon. In the presence of constant sources of heat and cold, the system can operate successfully without other energy costs. The operation of thermosyphons has a large literature (see, for instance, an overview in [3]). Most publications deal with the conditions of high thermal loads (100 W/m or higher per tube unit length), when the heat transfer is especially active [4]. However, the conditions of low thermal loads ($\leq$10 W/m) applied to the stabilization of permafrost, when the low kinetic energy of the two-phase flow hardly overcomes hydraulic resistance, have received much less attention. The action of the thermosyphons with the simplest construction (as vertical heat pipe) on permafrost is investigated mostly [5, 6]. The operation of some thermosyphon types, such as systems with horizontal evaporator tubes, has been poorly studied theoretically and experimentally. Nevertheless, such devices apply successfully on many constructions of northern areas [7–9].

To bridge the gap, model thermosyphons operated at low thermal loads, which simulate typical permafrost conditions, have been tested in the laboratory [10, 11]. Most thermosyphons used for thermal stabilization of permafrost run only during the cold season and are either vertical tubes or systems with horizontal evaporation tubes (HET). Fluid flow in such systems is commonly driven by gravity, as the use of capillary mechanisms has economic limitations. Where possible, the testing results are formulated as a boundary condition on the evaporator wall at the contact with the ambience, which allows exhaustive characterization of heat exchange between the system and the cooled natural or industrial materials and ensures correct formulation for the respective theoretical problem of external cooling.

2. Vertical thermosyphons

A vertical two-phase free convection system (thermosyphon) consists of relatively short (not over 10–15 m in length) tubes with an inner diameter of 30–50 mm [7, 12–14], based on Long's thermo-valve piling design [15]. The thermosyphons are inserted into the ground to most of their height and have a 1.5–2.0 m stick-up exposed to lower temperatures (**Figure 1**). Their operation commonly stops in summer, and special engineering solutions proceeding from thermal design are required to keep them running all year round or to increase the cooling effect (heat insulation, a certain number of tubes, etc.).

Two-phase free convention thermosyphons have been used to stabilize permafrost under kilometer-long aboveground pipelines (Trans-Alaska system or pipelines in northern, West, and Eastern Siberia), as well as buildings and utility structures in Russian Arctic oil and gas fields [13, 14, 16]. They are intended to cool down the ground to a designed temperature and keep this temperature stable for the whole lifetime of buildings and structures. Thermosyphons are most often installed prior to main construction, when foundations are being prepared. They are almost never used for the energy-consuming freezing of unfrozen parts of the ground, except for few cases of deeply buried systems for thermal stabilization of dam cores or for repairing thaw-related failures in the course of operation [8, 9].

The condenser can be equipped with heat absorption fins which are presumed to enhance the cooling effect, as it has been observed in practice. On the other hand, it follows from the theory [17] that fins should be mounted on the side of the medium with worse thermal properties. Special research is needed, however, to assess the potential efficiency of finning, given that heat transfer in thermosyphons is mainly
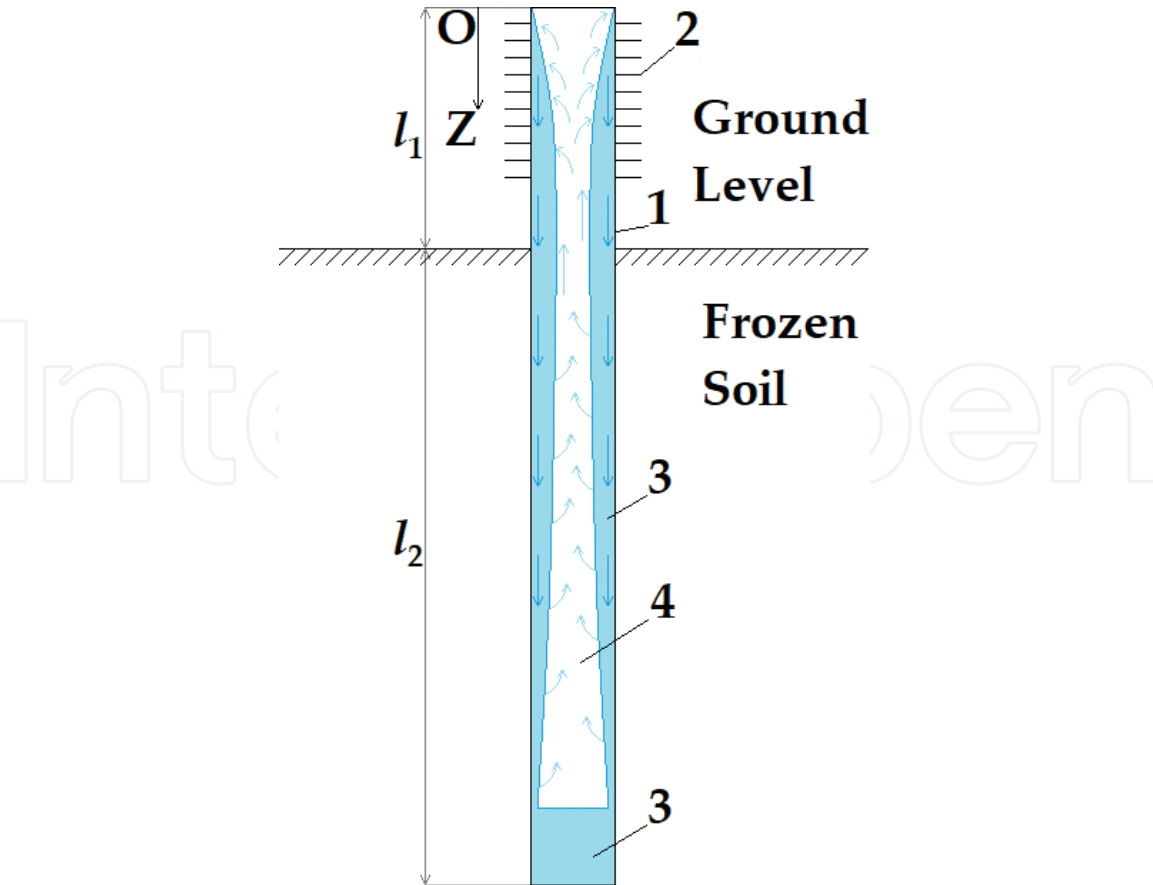
Figure 1.
A sketch of a two-phase thermosyphon: (1) tubular case, (2) fins, and (3 and 4) liquid and vapor phases of cooling fluid.

by convection above the ground and by conduction below the ground which has quite a low thermal conductivity. We have seen no evidence that would prove the thermal performance gain due specifically to fins.

2.1 Condenser

Heat transfer in thermosyphons is modeled jointly for processes inside (fluid phase change and flow) and outside (heat exchange with ground and air) such systems.

The two phases of the working fluid in the tube move as follows [1, 2]. The vapor pressure can be assumed constant along the tube length, which is short in our case, and the hydraulic resistance to vapor flow toward the condenser is very small. Correspondingly, the saturation temperature t_s (related to pressure via the saturation curve) is constant along both evaporator and condenser tubes. The condensed liquid flows along the inner tube as a thin film which thickens up progressively on its way to the evaporator. The film is the thinnest (zero) at the top of the condenser, is the thickest at the evaporator input, and then thins down upon evaporation while moving along the evaporator tube. In the simplest theoretical case, the hydraulic interaction of the two counterflowing phases can be assumed vanishing.

Heat exchange between the condenser and the air can be estimated easily [6, 18]. The total amount of heat Q_k dissipated from the condenser to air per unit time is related to the temperature difference $\Delta t_{ka} = t_k - t_a$ between the condenser wall (t_k) and the incoming air (t_a) as

$$Q_k = \alpha_{tot} \cdot S_k \cdot \Delta t_{sa} \tag{1}$$

$$\alpha_{tot} = \left(\frac{1}{\overline{\alpha_f}} \cdot \frac{S_k}{S_{ik}} + \frac{1}{\alpha_k} \right)^{-1} \tag{2}$$

$$\overline{\alpha_f} = \frac{\lambda_c}{\overline{\delta}}. \tag{3}$$

Note that equations for flat walls are used here and below, because the condensate film is very thin ($\delta \ll R$, where δ is the film thickness and R is the tube radius), according to observations on transparent physical models. In Eqs. (1)–(3), α_{tot} is the total effective heat loss; S_k is the total area of the condenser outer surface; S_{ik} is the total area of the condenser inner surface; α_k is the heat exchange between the condenser and the air, without the film thermal resistance (found using known relationships via heat exchange of the condenser wall with air [6]); $\overline{\alpha_f}$ is the average heat transfer across the film; $\overline{\delta}$ is the film thickness averaged over the condenser height; and λ_c is the condensate thermal conductivity. The thermal resistance of the condenser wall is neglected as it has quite a high thermal conductivity while the wall is thin.

The average heat transfer across the sinking condensate film $\overline{\alpha_f}$ can be found from known depth dependence of the film thickness $\delta(z)$. At a constant temperature of the condenser wall t_k, the depth-dependent film thickness $\delta(z)$ follows the Nusselt theory [19]. The equation for depth dependence of film thickness, corrected for heat exchange with air, neglecting vapor density (much smaller than liquid density) is given below for a condenser with the axis Oz directed down from the coordinates origin at the condenser top (**Figure 1**):

$$\int_0^z q(z)dz = \frac{\kappa \cdot g \cdot \rho_c}{3 \cdot \nu_c} \cdot \delta^3(z). \tag{4}$$

The heat flux density $q(z)$ at the condenser refers to its inner surface, of the area S_{ik}, and is

$$q(z) = \frac{\Delta t_{sa}}{\delta(z)/\lambda_c + S_{ik}/\alpha_k \cdot S_k}. \tag{5}$$

In Eqs. (4) and (5), ν_c and ρ_c are the kinematic viscosity and density of the condensate, respectively; κ is the heat of vapor-to-liquid phase transition; and g is the gravity acceleration.

Differentiation of both sides in expression (4) along z leads to the equation for $\delta(z)$, at $\delta(0) = 0$:

$$\frac{\nu_c \cdot \Delta t_{sa}}{\kappa \cdot g \cdot \rho_c} = \left(\frac{\delta(z)}{\lambda_c} + \frac{S_{ik}}{\alpha_k \cdot S_k} \right) \cdot \delta^2(z) \cdot \frac{d\delta}{dz}. \tag{6}$$

Integration of this equation leads to a biquadratic algebraic equation with respect to $\delta(z)$:

$$\delta^4 + \frac{4 \cdot \delta^3}{3} \cdot \frac{\lambda_c \cdot S_{ik}}{\alpha_k \cdot S_k} - \frac{4 \cdot \lambda_c \cdot \nu_c \cdot \Delta t_{sa} \cdot z}{\kappa \cdot g \cdot \rho_c} = 0. \tag{7}$$

The solution of Eq. (7) can be written in elementary functions, but it would be cumbersome and inconvenient for further analysis. A more simple relation can be obtained for the small film thickness, with the first term in Eq. (7) much less than the second one:

$$\delta \leq \leq \frac{4 \cdot}{3} \cdot \frac{\lambda_c \cdot S_{ik}}{\alpha_k \cdot S_k}. \tag{8}$$

As follows from the comparison of relations (8) and (5) (factor *4/3* being insignificant), the film thermal resistance becomes negligible when inequality (8) fulfills. It means that the performance of highly efficient condensers (with large S_c and high α_c, with a large dot product in the denominator of the right-hand side) is limited by the thermal resistance of the film, even commensurate with the resistance of the condenser. Therefore, the fulfillment of inequality (8) places constraints on the design of finned condensers in thermosyphons and in this respect is an economically and technologically important criterion. The respective requirement imposed on the condenser design has to be taken into account in further consideration.

With regard to the formulated requirement, we obtain the equation for the film thickness from Eq. (7), neglecting the first term in the left-hand side:

$$\delta(z) = \left(\frac{3 \cdot \nu_c \cdot \Delta t_{sa} \cdot z}{\kappa \cdot g \cdot \rho_c} \cdot \frac{\alpha_k \cdot S_k}{S_{ik}} \right)^{\frac{1}{3}}. \tag{9}$$

The film is the thickest on the condenser bottom, at $z = l_1$ (**Figure 1**). If inequality (8) fulfills at the maximum film thickness, it obviously fulfills for any thinner film. From relations (8) and (9), it follows that

$$\frac{\alpha_k \cdot S_k}{S_{ik}} \cdot \left(\frac{3^4 \cdot \nu_c \cdot \Delta t_{sa} \cdot l_1}{4^3 \cdot \lambda^3_{\,c} \cdot \kappa \cdot g \cdot \rho_c} \right)^{\frac{1}{4}} \leq \leq 1. \tag{10}$$

The left-hand side of inequality (10) is dimensionless and depends on the fluid (coolant) type, as well as on the condenser design. The inner and outer surface areas of an unfinned condenser are equal (the wall thickness being neglected), and the first factor in the left-hand side is equal to the heat loss α_a for unfinned (smooth-walled) tubes in the case of cross flow around tubes defined by the known relationship from the specified wind speed [20]. Let the left-hand side of inequality (10) be denoted as Φ with subscripts that refer to different coolants. For R = 16 mm, l_1 = 1.5 m, and the wind speed 3 and 8 m/s, the α_a values are 26.4 and 58.3 W/(m²·deg), while Φ values are Φ_{am} = 8.26 × 10⁻³, 1.83 × 10⁻² for ammonia, Φ_{fr-12} = 1.50 × 10⁻¹, 3.33 × 10⁻¹ for Freon-12, Φ_{fr22} = 1.04 × 10⁻¹, 2.31 × 10⁻¹ for Freon-22, Φ_{CO_2} = 2.63 × 10⁻², and 5.79 × 10⁻² for CO_2 (at the temperature difference about the maximum Δt_{sa} = 20°C). Thus, inequality (10) fulfills in all cases in the absence of fins (though not perfectly for Freons at high wind speed), and the contribution of film thickness can be neglected for all fluid considered above. On the other hand, fins on the outer surface of the condenser improve external heat exchange, but their enhancement loses sense when the thermal resistance of the film becomes significant.

For a finned condenser, the parameter Φ depends on thickness, spacing, and other parameters of fins (see the fin thickness dependence of Φ in **Figure 2** for different fluids but the same fin parameters and a wind speed of 5 m/s). For the chosen condenser design, inequality (10) fulfills well for all fin thicknesses with ammonia and slightly worse with carbon dioxide. With Freons, only very thin fins can be efficient, but they may be problematic to fabricate. The effect of the thermal resistance of a condensate film is controlled by its thickness and the thermal conductivity of the liquid phase in different coolants. Variations of film thickness at the condenser output as a function of fin thickness for ammonia and Freon-12
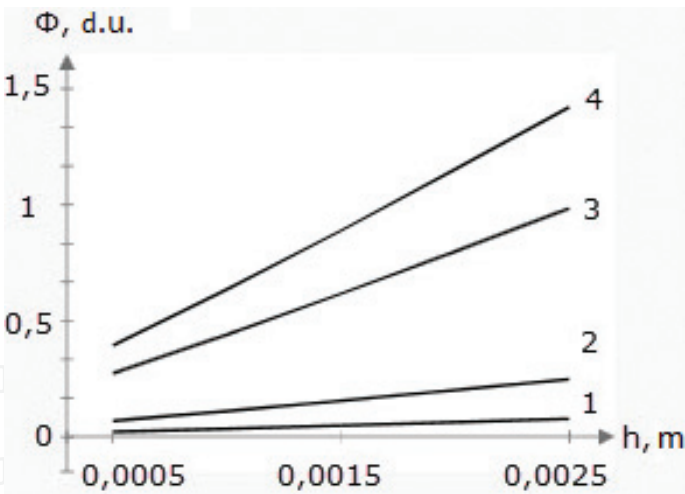
Figure 2.
Behavior of parameter Φ as a function of fin thickness (h) for ammonia (1), CO_2 (2), HCFC (Freon)-22 (3), and HCFC (Freon)-12 (4) fluids, at R = 16 mm and l_1 = 1.5 m.

(**Figure 3**) show that ammonia films are at least 5 times thinner, have about 8 times higher thermal conductivity, and, hence, have about 40 times lower thermal resistance.

As relation (8) fulfills, Eq. (2) for the total heat loss from the condenser becomes simpler:

$$\alpha_{tot} = \alpha_k. \tag{11}$$

2.2 Evaporator

The thickness of the sinking condensate film continuously decreases from the maximum δ_0 at the evaporator input, which coincides with that at the condenser output, and can be estimated by expression (9) at $z = l_1$. The depth-dependent film thickness variations in the evaporator likewise follow the Nusselt theory, applied to evaporation instead of condensation; at a constant temperature on the evaporator wall, t_g is equal to the current temperature of the ambient ground. The previously estimated [21] fluid flow rates inside the system largely exceed the rate of ground
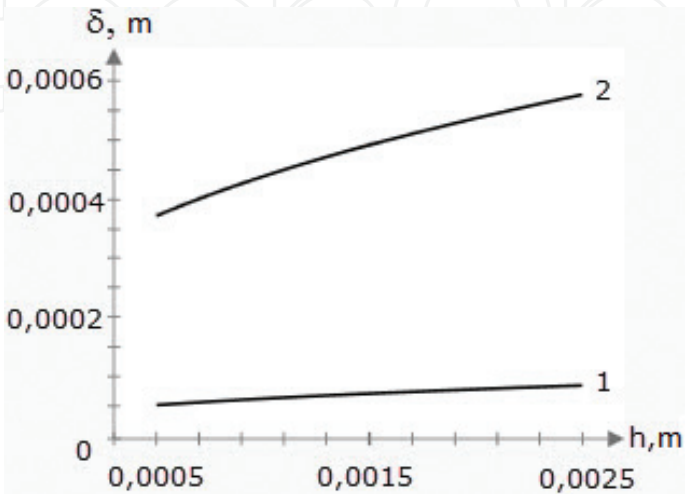

Figure 3.
Film thickness (δ) inside a condenser as a function of fin thickness (h) for ammonia (1) and HCFC (Freon)-12 (2) fluids.

temperature redistribution. Therefore, the formation and flow of the condensate film can be considered as a quasi-stationary process at the above conditions. In this case, the heat flux to the evaporator $q(z)$ is

$$q(z) = \frac{\lambda_c \cdot \Delta t_{gs}}{\delta(z)}. \tag{12}$$

The equation of the evaporator heat budget (similar to Eq. (4)) makes basis for the differential equation with respect to film thickness. With the initial condition $\delta = \delta_0$ at $z = l_1$, the equation for $\delta(z)$ becomes

$$\delta^4(z) = \delta_0^4 + \frac{4 \cdot \lambda_c \cdot \Delta t_{gs} \cdot \nu_c \cdot (l_1 - z)}{\kappa \cdot \rho_c \cdot g}; l \geq z \geq l_1, \tag{13}$$

where l is the total tube length. According to expression (13), the nonzero film thickness is limited by some natural depth reasonably corresponding to the maximum evaporator length (see below).

Eq. (13), with averaging along z, can be used to calculate the average heat loss over the evaporator $\overline{\alpha}_{if}$. Note that the parameters t_s and t_g remain unconstrained in all above equations. The saturation temperature t_s is estimated using the total heat budget for the system as a whole; heat coming to the evaporator equals that dissipating to the air from the condenser; $Q_k = Q_f$, where Q_k is defined by relation (1), while the heat from the evaporator is $Q_f = \overline{\alpha}_{if} \cdot S_f \cdot \Delta t_{gs}$ (where the evaporator surface area $S_f = 2 \cdot \pi \cdot R \cdot l_2$ and its length is l_2). Solving the heat budget equation with respect to t_s gives

$$t_s = \frac{S_f \overline{\alpha}_{if} \cdot t_g + S_k \cdot \alpha_k \cdot t_a}{S_f \overline{\alpha}_{if} + S_k \cdot \alpha_k}. \tag{14}$$

With Eqs. (12) and (13), the average heat loss from the evaporator $\overline{\alpha}_{if}$ likewise depends on the temperature t_s and is given by

$$\overline{\alpha}_{if} = \left(\frac{\lambda_c^3 \cdot \kappa \cdot \rho_c \cdot g}{4 \cdot \nu_c \cdot l_2 \cdot \Delta t_{gs}} \right)^{0.25}. \tag{15}$$

To write the equation for t_s, we first define the difference $\Delta t_{gs} = t_g - t_s$ using expression (14), then pick the terms with the difference Δt_{gs}, and obtain the transcendent algebraic equation with respect to this value:

$$\Delta t_{gs} + \frac{3}{4} \cdot \frac{S_f}{\alpha_k \cdot S_k} \cdot \left(\frac{\lambda_c^3 \cdot \kappa \cdot \rho_c \cdot g}{4 \cdot \nu_c \cdot l_2} \right)^{0.75} \cdot \Delta t_{gs}^{0.75} = \Delta t_{ga}, \tag{16}$$

which is solved numerically. In the range of ground temperatures t_g from 0°C to t_a, the temperature t_s is close to t_g to thousandth fractions for ammonia and 0.6°C for Freon-12.

The difference Δt_{gs} becomes important for estimating the maximum length l_2^* of the evaporator tube and cannot be neglected. At $\delta = 0$, the maximum tube length is obtained from expression (13) as

$$l_2^* = \delta_0^4 \cdot \frac{\kappa \cdot \rho_c \cdot g}{4 \cdot \lambda_c \cdot \Delta t_{gs} \cdot \nu_c}. \tag{17}$$

Let the heat loss from the condenser in Eq. (9) be $\alpha_k \cdot S_k / S_{ik} \equiv F$ (see its behavior as a function of fin thickness in **Figure 4**) with the values 40, 200, and 400 W/(m^2·deg). Then, $l_2^* = 1.7$, 6.0, and 11.9 m, respectively, for ammonia and can reach 200 m for Freon-12. This length may be a major advantage of Freon evaporators in thermosyphons used for cooling deep ground.

In principle, evaporator tubes in thermosyphons used in deep ground can be longer than the estimated maximum value, but they should be filled with liquid coolant till the upper limit. In this case, heat transfer should be considered with regard to a shift in the temperature of boiling (in the lower tube section) under the effect of hydrostatic pressure. However, we have no reliable evidence of thermosyphon operation in these conditions.

The reported estimates for the maximum evaporator length require further experimental checks. The issue is especially important because one of us repeatedly observed sporadic ebullition of fluid at the evaporator bottom during laboratory testing of vertical thermosyphons in physical models with transparent walls. The vapor-liquid flow from such ebullition wets the evaporator walls and reaches the condenser, while the evaporator temperature falls abruptly, and moisture condenses on its outer wall surfaces. This effect, which may play a significant role, was demonstrated in a video at TICOP [22], but it is neglected in this consideration. Laboratory testing of thermosyphons has to be continued. The sinking film moves wavelike upon interaction with the down-going flow of vapor [23], but the wavelike flow is stable and even improves the heat exchange to some extent [19].

2.3 External problem for thermal stabilization

The distribution of ground temperatures in the zone of thermal stabilization is estimated as follows. The key issue is to constrain the boundary conditions on the evaporator outer wall which contacts the ground. For this, the saturation temperature (t_s) is expressed from the equation of total heat budget. The heat loss from the condenser Q_k is defined by the same Eq. (11), while the heat coming to the evaporator Q_f from the ground is

$$\alpha_k \cdot S_k \cdot \Delta t_{sa} = S_f \cdot \lambda_f \cdot \left(\frac{\partial t}{\partial r}\right)_R, \tag{18}$$
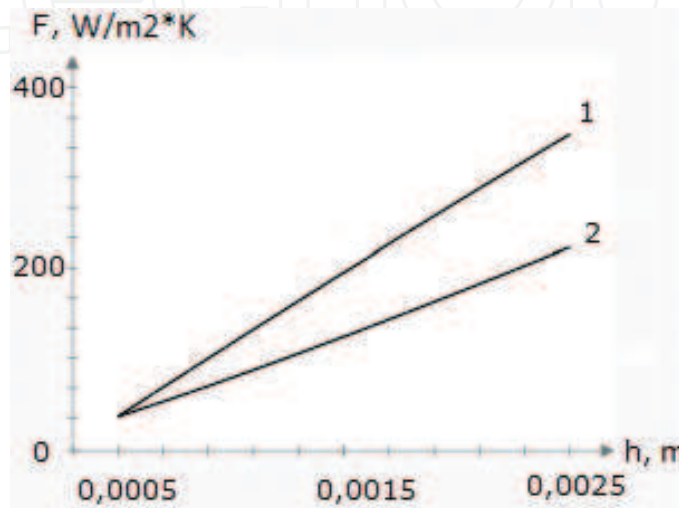

Figure 4.
Behavior of parameter F as a function of fin thickness (h); R = 16 mm.

where λ_f is the thermal conductivity of frozen ground and t is the ground temperature depending on the radial coordinate r (in the axisymmetric case) and the time τ. With the Eq. (14) for t_s and inequality (8), the sought condition is

$$\frac{\alpha_k \cdot S_k}{S_f} \cdot (t_a - t_g) = -\lambda_f \cdot \left(\frac{\partial t}{\partial r}\right)_R.$$ (19)

The same equation was obtained earlier for an unfinned condenser [21], with the only difference in the factor F in the left-hand side of condition (19), before the temperature difference (in the absence of fins, $F_{tot} = \alpha_a l_1/l_2$). Eq. (19) is a third-order boundary condition on the evaporator outer wall ($t_g \equiv t(R)$), which fully characterizes the cooling effect in problems for temperature variation in permafrost stabilized by vertical thermosyphons. The condition allows formulating and solving a large scope of problems concerning the temperature field maintained with any number of vertical thermosyphons in construction. This is the most important result of this part.

3. HET systems

Thermosyphons with horizontal evaporation tubes allow using pad foundations instead of piling in some types of structures, which saves labor costs. These systems have been largely used for permafrost stabilization in terms of works designed mainly by the R&D companies *Fundamentstroiarkos* (direct-flow HET systems) and *Fundamentproekt* (counter-flow systems with inclined evaporator tubes) [8, 24], but no methods are still available for estimating their efficiency. The known theoretical studies characterize the operation of HET systems at high thermal loads of tens or hundreds W/m [4], while the loads in thermal stabilization of permafrost do not exceed 3–5 W/m [11]. As shown by laboratory testing at small thermal loads [10, 11], the two phases of the working fluid have commensurate volumetric contents along the tube length and interact mechanically. This fact does not allow simple description of fluid dynamics and heat exchange in the two-phase flow (e.g., [25–28]). A pure theoretical description of these processes is hardly possible at the time being and requires updating with reference to testing results for specific systems. The original design of HET systems implied unidirectional flow of both phases all along the tubes, which reduces hydraulic resistance to the coolant motion and improves the system performance.

3.1 Methods and results of laboratory testing

The operation of a laboratory model of an HET system is discussed below for a general experiment layout as in **Figures 5** and **6**. The laboratory model was described in detail earlier [10, 11]. The test equipment includes temperature sensors (thermistors), an electronic vacuum meter, a level gauge, and an automatic recorder (**Figure 5**). The condenser is made of metal and placed in a large cooling chamber, while the evaporator consists of glass tubes connected by chemically inert rubber hoses and laid horizontally on wooden pads on the room floor. The transparent glass tubes make visible the flow behavior in different segments of the system, which is important for documenting its operation. Acetone was used as a cooling fluid as its saturation vapor pressure is below the ambient pressure within the applied temperature range (unlike most coolants used in the industry). This ensures cheap, straightforward, and safe handling of the model but requires
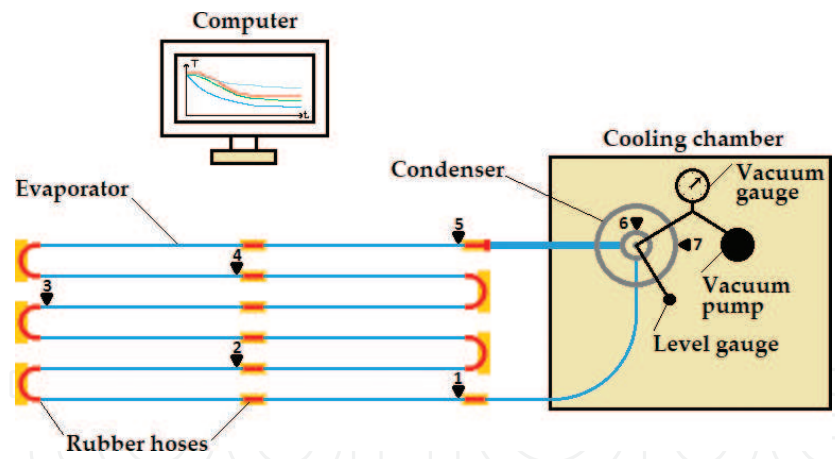
Figure 5.
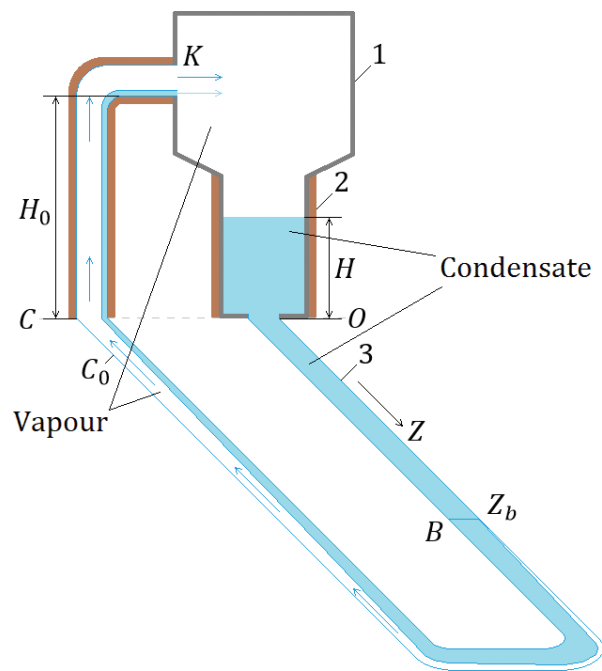*A sketch of a laboratory test equipment. 1–7 are thermistors.*

Figure 6.
Structural scheme of the model system (symbols are explained in the text).

pumping out atmospheric gases which are present inside the system and interfere with its work.

The model of the HET system (**Figure 6**) consists of a condenser (1) with a narrower bottom part which accommodates the condensed liquid (2) and an evaporator (3). The vertical evaporator segment leading to the condenser input (segment CK in **Figure 6**) is made of a nontransparent insulating material, which masks the fluid flow. The flow behavior within this segment can be judged from examination of the neighbor glass horizontal segment C_0C inside the cooling chamber. When the system operates normally, both fluid phases flow in the same direction, toward the condenser input K, while the share of vapor is quite large. The flow of each phase toward point C within the main tube length undergoes successively the plug, wave, and projectile regimes.

The system operates normally as long as the tube length-to-diameter (L/D) ratio remains ˜500 (in industrial systems, it may reach 5000 or more). As this ratio increases, the operation becomes progressively less stable, while the cooling effect (temperature difference between the evaporator and the room air) reduces. On the other hand, some amount of condensate liquid always flows back into the

evaporator during the normal operation. This return flow is visible from outside the cooling chamber [11], except for the nontransparent segment C_0C, and thus forms apparently all along C_0CK (**Figure 7**). The evaporator cools down till the lowest temperature during normal operation, which is recorded by thermistors (**Figure 8**) as distinct from the unstable one (**Figure 9**). The flow of phases within segment C_0C at normal (stable) regime can be either laminar or turbulent (**Figures 10** and **11**).

During the unstable operation, till failure, the liquid phase moves very slowly (visually seeming immobile) within the segment C_0C, while the vapor phase is restricted to bubbles of different sizes (**Figures 12** and **13**) which move relatively slowly toward the condenser input. The cooling effect in this case is often oscillatory and fails to reach the designed temperature at the normal regime (**Figure 9**).
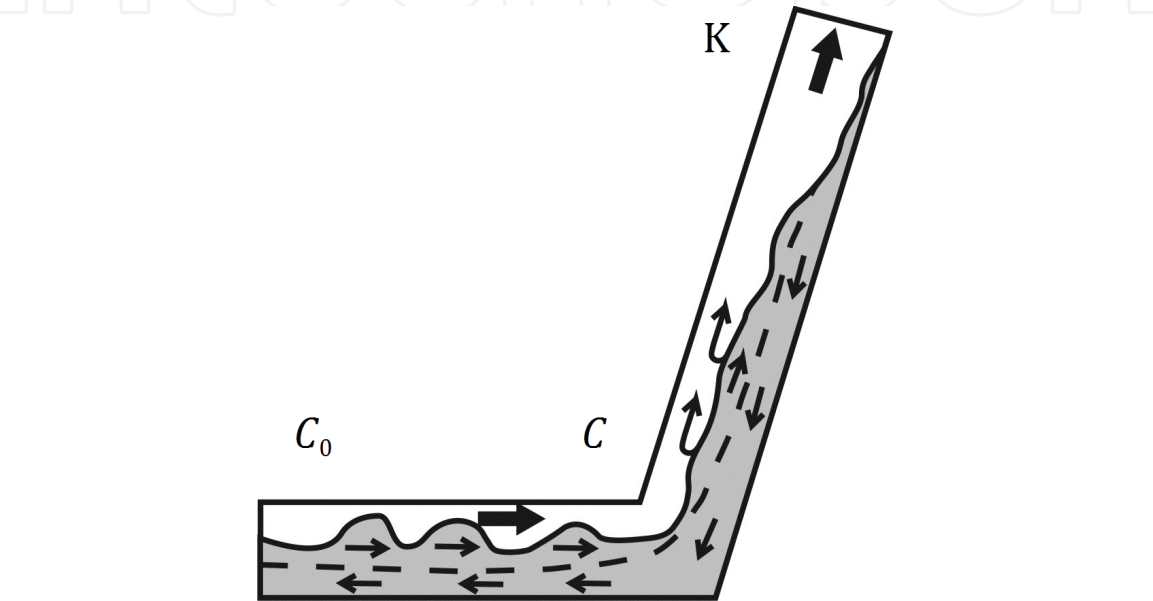
Figure 7.
Two-phase flow near the condenser input (segment C₀CK): Dark and light shades are condensate and vapor; heavy and thin arrows show vapor and liquid flows, respectively; dash line is the boundary between the two flows.
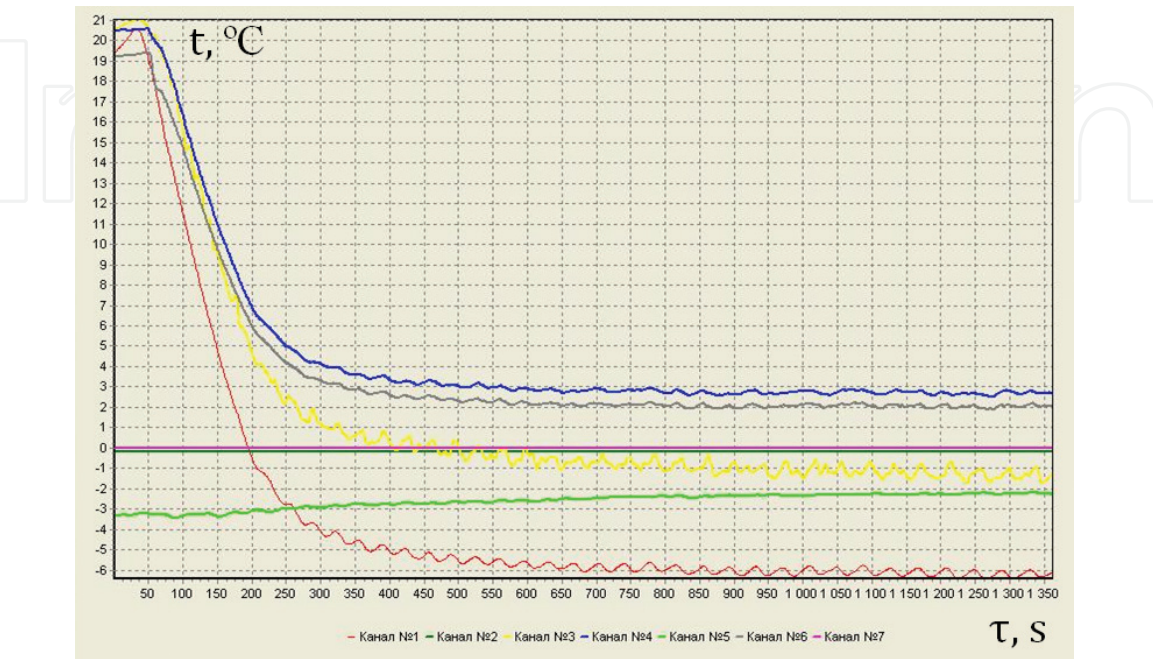

Figure 8.
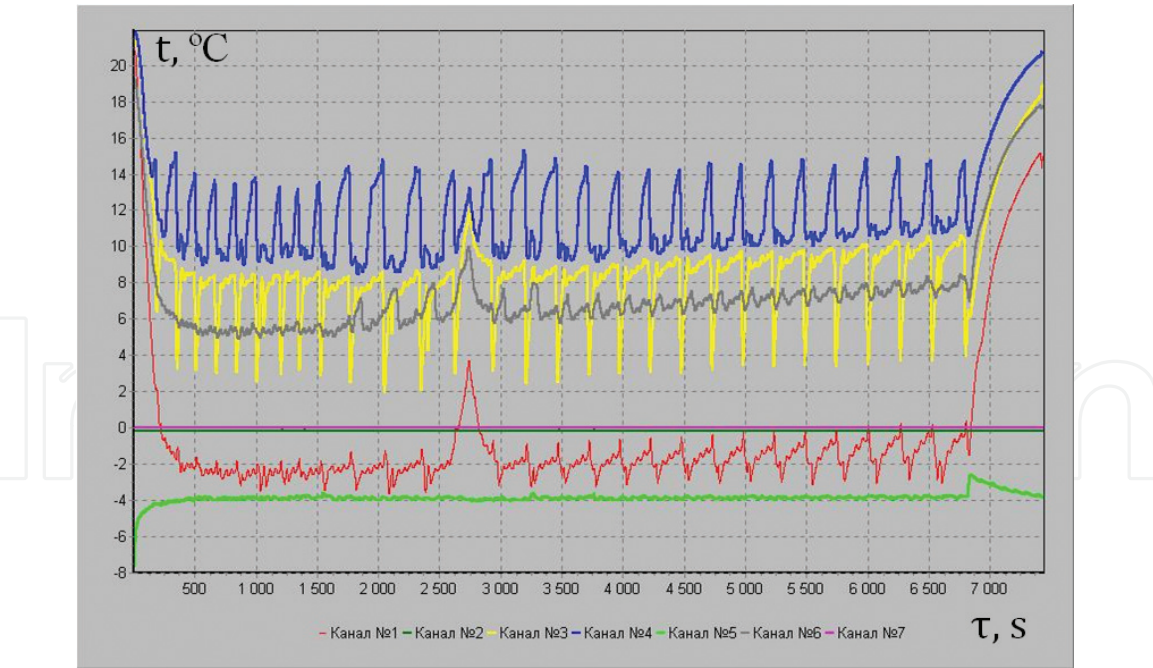*Thermistor readings along the evaporator tube at stable operation of the system.*

Figure 9.
Thermistor readings along the evaporator tube at unstable operation of the system.
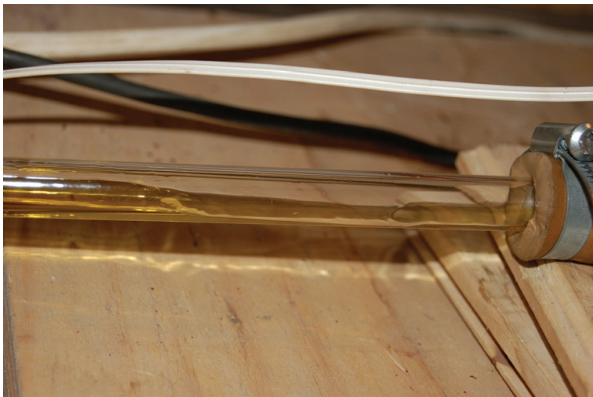

Figure 10.
Laminar flows within segment C_oC at stable operation.
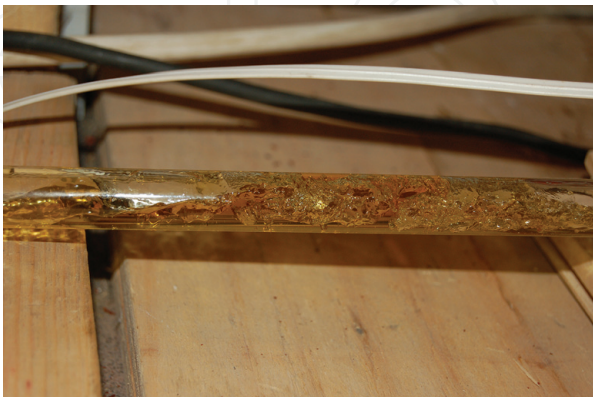

Figure 11.
Turbulent flows within segment C_oC at stable operation.

Cooling is the weakest at the smallest amount and slowest flow of vapor within C_0C, that is, the system actually fails. In this case, the condensate level H in the condenser (**Figure 6**) reaches its maximum [11], and constant return flow is visible from outside the evaporator, like during the normal operation. Thus, the return
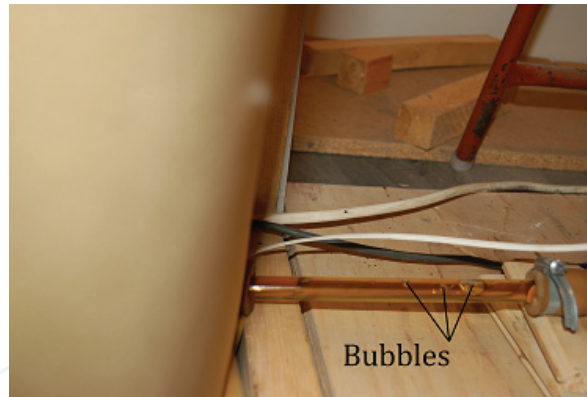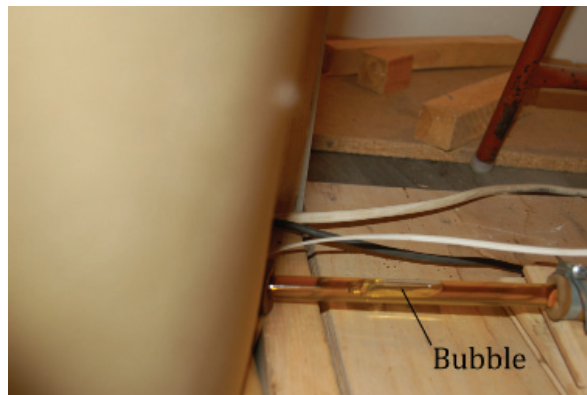
Figure 12.
Small vapor bubbles at unstable operation.

Figure 13.
Big vapor bubbles at unstable operation.

flow along C_0CK is a typical feature of fluid behavior (at least at small thermal loads on the evaporator). Other features (operation instability, slow start, poor cooling effect) become more prominent at longer evaporator tubes (greater L/D ratios) but are minor at short tubes.

The evaporator tubes of full-size HET systems are commonly fully filled with the liquid phase, while the condenser is filled partly, till the specified level H (relative to the evaporator position in the horizontal plane). However, the effect of the fluid volume on the system performance at small thermal loads remains poorly investigated. On the other hand, systems with a lower fluid volume are cheaper and pose lower hazard to environment in case of emergency spilling. The respective laboratory tests were performed also with a partly filled evaporator and an empty condenser ($\beta = L_0/L < 1$, where L_0 is the tube length filled with condensate and L is the total tube length), in order to initially increase the vapor share in the vapor–liquid mixture and thus reduce the hydraulic resistance and improve the system performance. The measured stationary temperature distribution along the tube for different H levels (**Figures 14–17**) demonstrates that the cooling effect reduces notably as the fluid volume increases.

Main testing results can be summarized as follows: (i) there is always a return flow of liquid sinking into the evaporator opposite to the main flow of the two-phase mixture in the segment near the condenser input (segment C_0CK in **Figure 6**) [11]. The presence of this return flow differs the real fluid behavior from the theoretical idea of unidirectional flow of the fluid phases along the whole circulation path (at least for small thermal loads); (ii) at low thermal loads, the systems with return flow develop a slug and plug regime that leads to failure [25]. Specifically, the condensate plugs increase the hydraulic resistance and obstruct the flow to the
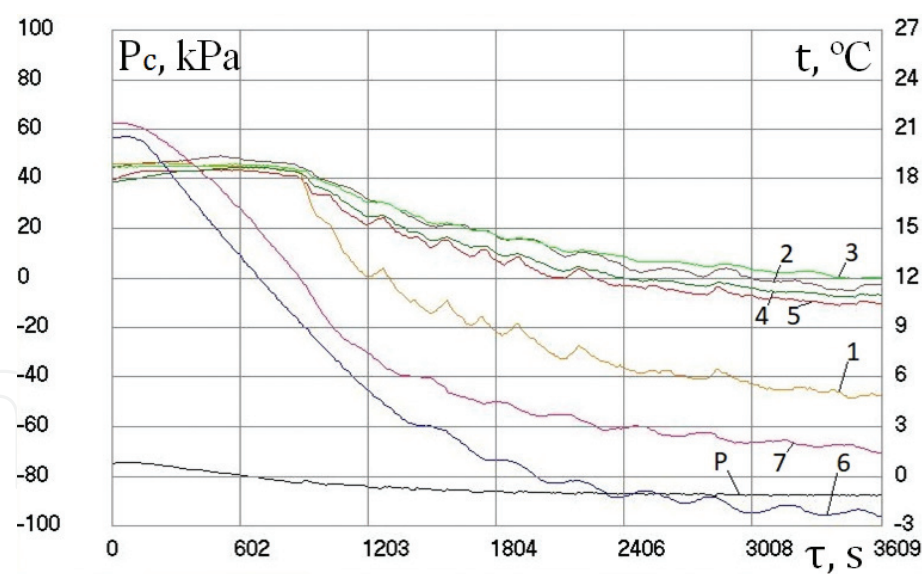
Figure 14.
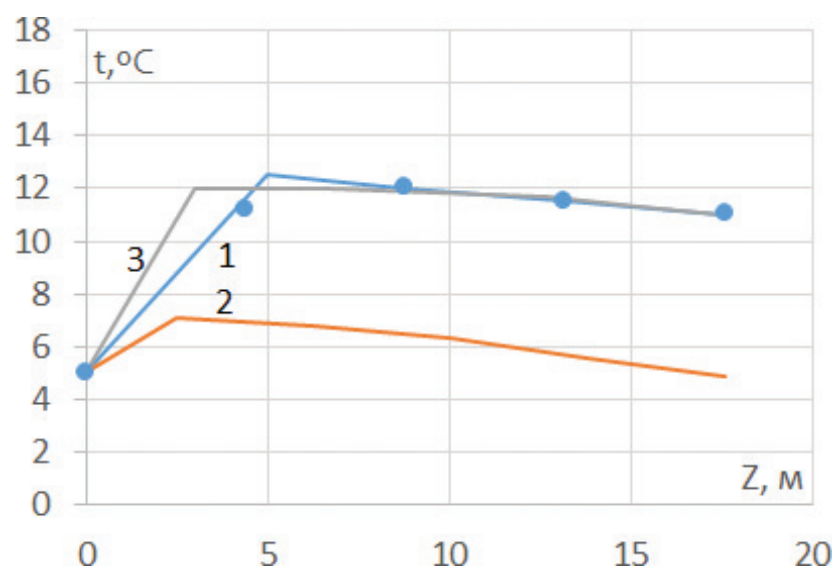*Temperatures at thermistor points (1–7) and excess pressure (P) during the operation of the model at β = 0.5.*

Figure 15.
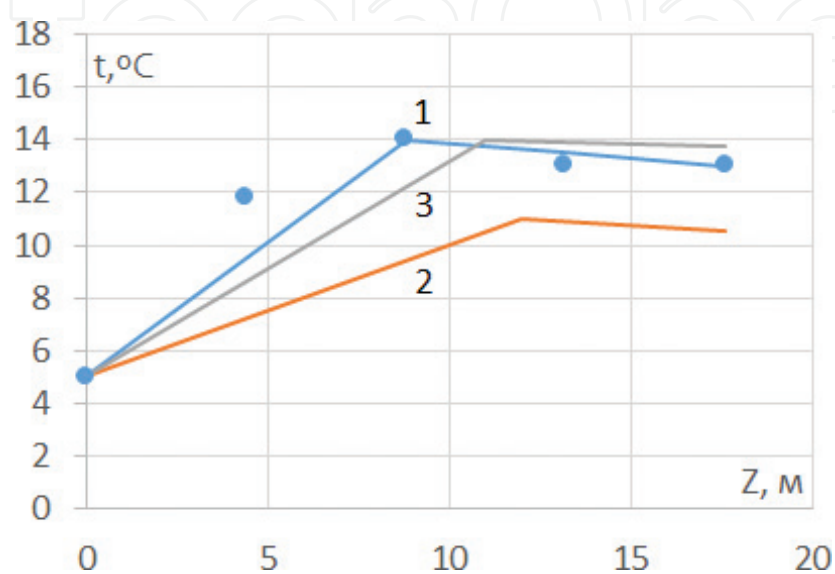*Measured (1) and calculated (2, 3) temperatures along the tube at β = 0.5, ω = 1 (2), and ω = 50 (3).*

Figure 16.
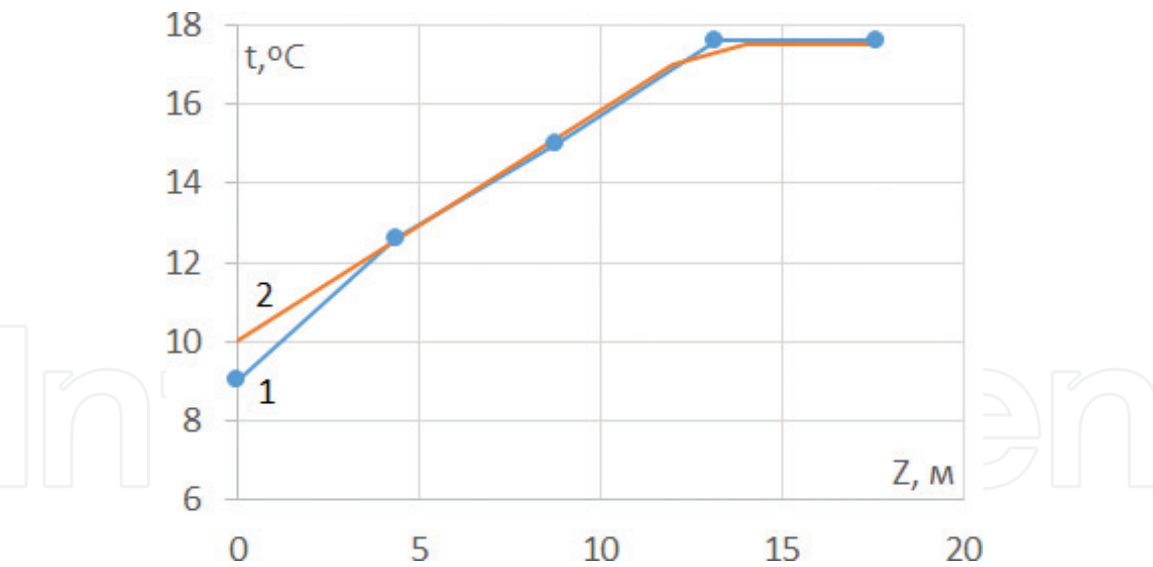*Measured (1) and calculated (2, 3) temperatures along the tube at β = 1.0, ω = 1 (2), and ω = 70 (3).*

14

Figure 17.
Measured (1) and calculated (2) temperatures along the tube at standard H level; ω = 1 (2).

condenser within this segment. The flow behavior may change frequently within a single test, which leads to oscillations of the evaporator temperatures (**Figure 9**). This fluid flow behavior at small thermal loads has to be taken into account in calculations for estimating the system performance.

The experimental uncertainty analysis of the experimental data was not done yet. It is planned for the next publications.

3.2 Calculations for thermosyphon design

According to the existing methods of fluid-dynamic calculations [25–28], the state of a two-phase flow in each tube cross section depends on the flow rates of vapor $G_w(z)$ and condensate $G_l(z)$, in kg/s and volumetric vapor content $\alpha_w(z)$, where z is the coordinate along the evaporator tube, with the origin at point O (**Figure 6**). The condensate flow rate is expressed via the total flow rate G: $G_l(z) = G - G_w(z)$. In the stationary process, G is constant along the flow, but it is unknown a priori and has to be calculated.

The function $\alpha_w(z)$ in the simplest model of Lockhart-Martinelli [26, 27] is defined by $G_w(z)$ and $G_l(z)$. The fluid flow along the tube is split into two parts: heating and two-phase flow. In the heating part, from the point O to the boiling point B at z_b (**Figure 6**), $\alpha_w(z) = 0$, and the coordinate z_b is found from the known solutions for temperature and pressure for the single-phase flow at a given lateral heat transfer and from the condition at which the flow parameters reach the fluid saturation at the given point. In the simplest case of constant heat flux q along the evaporator wall (W/m), the temperature change between O and z_b is

$$t(z) = t_s + q \cdot z / G \cdot c_l, \qquad (20)$$

where t_s and c_l are the fluid temperatures at the output of the cooling chamber (point O, **Figure 6**) and the specific heat of the liquid phase, respectively. At the liquid–vapor equilibrium, the saturation pressure P_s correlates with the temperature of the phases t, and the $P_s(t)$ function can be determined empirically as a three-parameter curve, to a sufficient accuracy. Here we use the quadratic equation:

$$P_s(t) = b_1 + b_2 \cdot t + b_3 \cdot t^2, \qquad (21)$$

with the coefficients $b_1 = 10^4$ *Pa*, $b_2 = 600$ *Pa/°C* and $b_3 = 12.5$ *Pa/(°C)^2* for an acetone fluid. The z-dependent saturation pressure can be expressed as in Eq. 20: $P_s(z) = P_s(t(z))$. The liquid flow within the *OB* segment is laminar, and expression for hydrodynamic pressure $P_h(z)$ is given by

$$P_h(z) = P_k + \rho_l \cdot g \cdot H - \frac{128 \cdot \mu_l \cdot G \cdot (H + z)}{\pi \cdot \rho_l \cdot D^4},$$ (22)

where $P_k = P_s(t_k)$; t_k and P_k are, respectively, the pressure and temperature of saturation vapor inside the condenser; ρ_l and μ_l are the density and dynamic viscosity of the condensate; and D and g are the inner diameter of the tube and the acceleration due to gravity. The position of the boiling point B (z_b) is found from the equation $P_s(z) = P_h(z)$ (the respective equation is omitted). Both t_k and P_k inside the condenser are a minimal value of temperature and pressure for all two-phase segment *BCK*.

In the two-phase flow part, between z_b and the condenser input K (**Figure 6**), the functions $G_w(z)$ and $\alpha_w(z)$ increase monotonically from zero at z_b, while the z dependence is calculated according to the specified conditions of heat transfer on the evaporator wall. In the current model, all incoming heat is spent on fluid evaporation, and $G_w(z)$ is

$$G_w(z) = q(z - z_b)/\kappa.$$ (23)

Note that all variables depend on G, H, H_0, and other constructive and external parameters (e.g., on the temperature in the cooling chamber t_a). The pressure gradient within the two-phase flow segment dP/dz is a sum of three components (see [27, 28] for their expressions), $dP/dz = (dP/dz)_f + (dP/dz)_a + (dP/dz)_g$, which refer to friction, flow acceleration, and gravity, respectively. The gravity component disappears within the horizontal tube, and the acceleration component disappears within the vertical tube segment *CK* (with the assumption of ideal insulation of the inlet tube). Integration of the dP/dz equation along the segment between the condenser top (where the pressure is P_k) and condenser input K leads to zero total pressure, and the sought variables can be found by equation

$$\oint \frac{dP(z, G, H)}{dz} dz = 0.$$ (24)

In this equation, P depends explicitly on the parameters G and H, which is relevant to the further consideration. The variables t_k and t_s in Eqs. (20) and (22) can be found from the equation for condenser-air heat exchange (with regard to the condenser design and processes inside it) and the integral balance equation for the stationary operation of the system (similar to Eq. (14). In this consideration though, focused on the applicability of the existing calculation methods to small thermal loads, the temperatures are found in a simpler empirical way: from thermistor readings (#1 and #7 in **Figure 5** for t_s and t_k, respectively).

If the condenser design ensures invariable H at any change inside the evaporator during the system operation (i.e., H is a specified and known value in the calculations), Eq. (24), together with known t_s and t_k, is sufficient to find all process parameters. In this case, integration in relation (24) leads to an algebraic equation with respect to G which has a simple numerical solution. Once G has been found, all flow parameters can be found as well: z_b, $G_w(z)$, $\alpha_w(z)$, $P_s(z)$, and the temperature distribution within the two-phase flow part which is related with the saturation pressure $P_s(z)$ as in expression (21). The temperature distribution along the tube

should be a continuous function of z, given the way of z_b determination. It is convenient in our case to divide the friction contribution to the integral of Eq. (24) into two components (I_{fL} from the origin to C_0 and I_{fH0} along C_0CK), as high hydraulic resistance within C_0CK is especially important for this consideration.

If the evaporator tube is filled to a part of its length ($\beta \leq 1$), the initial fluid level is $H = 0$, while H is set unprompted and is unknown (to be calculated) in operant condition. For this, an additional equation is used, which is a mathematical form of the mass conservation law for fluid in the system, likewise including two unknowns (G and H), assuming equal tube diameters:

$$(1 - \beta) \cdot L + (1 - \alpha_w(L)) \cdot H_0 + H = \int_{z_b}^{L} \alpha_w(z)dz, \qquad (25)$$

where z_b and $\alpha_w(z)$ parametrically depend on G and H. Thus, Eqs. (24) and (25) make up a system of algebraic equations with respect to G and H. Solving them jointly yields the unknowns and the temperature along the tube at arbitrary external parameters (temperature in the cooling chamber, heat transfer at the evaporator wall, fluid properties, and system specifications). Cooling of the evaporator relative to its ambience (room air in the case of laboratory testing) is the main parameter of its heat exchange with the host material.

3.3 Calculated and measured data compared

The calculated and measured data can be compared with an example of three laboratory tests at $\beta = 0.5$, $\beta = 1$, and at a standard fluid level ($H = 1.6\ m$). Other experimental conditions are identical: cooling chamber temperature $t_c = -12.5°C$ and room air temperature $t_a = +23°C$, $L = 17.6\ m$, and $D = 0.01\ m$ ($L/D \sim 2000$). The thermal load on the evaporator is assumed to be $q = 2.8\ W/m$ proceeding from free convection as the basic mechanism of heat exchange between the evaporator and the ambient air. Time-dependent temperature variations recorded by all thermistors and saturation pressure for the run with $\beta = 0.5$ (**Figure 14**) allow estimating the values $t_k = 1.5$ and $t_s = 5$ (°C) in the case of a quasi-stationary process (similar records for the other runs are not shown). The measured evaporator temperatures for the quasi-stationary process approximated by curve 1 in **Figure 15** differ markedly from those calculated (curve 2) with Eqs. (24) and (25). To improve the fit, the calculated values require correction by a factor of ω (at the integral I_{fH0}), which increases hydraulic resistance within the segment C_0CK. A good fit between measured and calculated temperatures can be achieved with a 50 times higher hydraulic resistance or at $\omega = 50$ (curve 3). In the second run ($\beta = 1.0$, **Figure 16**), the fit improves at $\omega = 70$. This correction for higher hydraulic resistance within the segment C_0CK is valid for partly filled evaporators with the filled-to-total tube length ratios (β) from 0.3 to 1.0. According to preliminary estimates, the correction factor ω in this β range can vary from a few to hundreds of times, depending on variations of other parameters. In the case of standard H level (run 3, **Figure 17**), the fit is good without correction ($\omega = 1$).

4. Conclusions

Improving the performance of vertical thermosyphons by increasing the surface area of fins is limited by the internal thermal resistance of the condensate film that sinks down the condenser inner walls. The thermosyphon-ground heat exchange

can be described by the third-order boundary condition, with the respective problem formulation.

Laboratory testing shows that the model of an HET system in the tested design can operate with both partly and fully filled evaporator tubes. The calculations in the former case should additionally include the mass conservation equation for the working fluid. Calculated and measured data fit well with a correction for higher hydraulic resistance in the flow along the vertical evaporator segment leading to the condenser input. The modified calculations remain semiempirical through and require further updating.

Acknowledgements

Notes

Author details

Yakov B. Gorelik* and Artur H. Khabitov
Earth Cryosphere Institute, Siberian Branch of the Russian Academy of Sciences, Russia, Tyumen

*Address all correspondence to: gorelik@ikz.ru

IntechOpen

References

[1] Dunn PD, Reay DA. Heat Pipes. Oxford: Pergamon Press; 1978. p. 334

[2] Pioro IL, Antonenko VA, Pioro LS. Efficient Heat Exchange Systems with Two-Phase Thermosyphons. Kiev: Naukova Dumka; 1991. p. 246 (in Russian)

[3] Vasil'ev LL, Konev SV. Heat pipes. Heat Transfer (Soviet Research). 1974;**6**(1):1-105

[4] Kutepov AM, Sterman AS, Stiushin AG. Fluid Dynamics and Heat Transfer in Vapor Formation. Moscow: Vysshaya Shkola; 1986. p. 448 (in Russian)

[5] Khrustalev LN. Principles of the Geotechnics at Cryolithozone. Moscow: MSU; 2005. p. 554 (in Russian)

[6] Gorelik JB, Seleznev AA. Efficiency of finning in short vertical two-phase thermosyphons for construction on permafrost. Earth's Cryosphere. 2016;**XX**(2):78-89

[7] Dolgikh GM, Okunev SN. Construction and stabilization of cooled foundations in permafrost by *Fundamentstroiarkos* company. In: Proceedings of the International Conference on Theory and Practice of Permafrost: Assessment and Predictions; 29-31 May 2006; Russia. Tyumen: TNGGU; 2006. pp. 228-232

[8] Dolgikh GM, editor. Systems for Thermal Stabilization of Permafrost. A Collection of Papers by Specialists from *Fundamentstroiarkos* R&D Company for 2010–2014. Novosibirsk: Geo; 2014. 218 p (in Russian)

[9] Kutvitskaya NB, Minkin MA. Design of foundations for infrastructure of oil, gas, and condensate field in complex permafrost conditions. Osnovaniya, Fundamenty, Mekhanika Gruntov. 2014;**1**:21-25

[10] Gorelik JB, Gorelik RJ. Laboratory research of work of the natural convectional biphase cooling device with horizontal evaporative part. Kriosfera Zemli. 2011;**XV**(2):34-43

[11] Gorelik JB. Operation of two-phase thermosyphons with horizontal evaporator tubes: Causes of instability. Earth's Cryosphere. 2015;**XIX**(4):81-93

[12] Vasil'ev LL, Vaaz SL. Freezing and Heating of Ground with Thermosyphons. Minsk: Nauka i Tekhnika; 1986. 192 p (in Russian)

[13] Vyalov SS, editor. Ground Temperature Stabilization with Thermosyphons. Yakutsk: IM SO RAN; 1983. 124 p (in Russian)

[14] Makarov VI. Thermosyphons in High-Latitude Construction Engineering. Novosibirsk: Nauka; 1985. 169 p (in Russian)

[15] Long EL. Means for Maintaining Permafrost Foundations. Patents USA, Cl. 165–45; 1964. No. 3, 217, 791

[16] Dolgikh GM, Dolgikh DG, Okunev SN. Freezing of soils: Engineering solutions of *Fundamentstroiarkos* company. In: Proceedings of the International Conference on the Cryosphere of Petroleum Provinces; 26-28 May 2004; Russia. Tyumen: TNGGU; 2004. pp. 56-57

[17] Arnold LV, Mikhailovskiy GA, Seliverstov VM. Engineering Thermodynamics and Heat Transfer. Moscow: Vysshaya Shkola; 1979. p. 445 (in Russian)

[18] Roizen LI, Dulkin IN. Thermal Design of Finned Surfaces. Moscow: Energiya; 1977. p. 255 (in Russian)

[19] Mikheev MA, Mikheeva IM. Fundamentals of Heat Transfer.

Moscow: Energiya; 1973. 320 p (in Russian)

[20] Wong HY. Handbook of Essential Formulae and Data on Heat Transfer for Engineers. London, New York: Longman Group Ltd; 1977. p. 236

[21] Gorelik JB. Modeling ground temperature field around vapor-liquid thermal piles. Problemy Nefti i Gaza Tyumeni. 1980;**47**:58-61

[22] Gorelik JB. Laboratory study of the devices for thermostabilization of frozen ground. Initiative oral reporting. In: Program of 10th International Conference on Permafrost (TICOP); 25-29 June 2012; Russia. Salekhard: Pechatnik; 2012. p. 18

[23] Kapitsa PL. Wave flow of thin liquid layers. Zhurnal Teoreticheskoy Fiziki. 1948;**18**(1):3-18

[24] Minkin MA. Basements and Foundations in Permafrost. Moscow: GASIS; 2005. 213 p (in Russian)

[25] Wallis G. One Dimensional Two-Phase Flow. New York: McGraw-Hill; 1969. p. 440

[26] Butterworth D, Hewitt GF. Two-Phase Flow and Heat Transfer. Oxford University Press (Harwell Series); 1977. 514 p

[27] Crowe CT, editor. Multiphase Flow Handbook. London—New York: Taylor & Francis; 2006. 1128 p

[28] Labuntsov DA, Yagov VV. Mechanics of Two-Phase Systems. Moscow: MEI; 2000. 374 p (in Russian)